CMS Physics Analysis Summary

Contact: cms-pag-conveners-susy@cern.ch 2016/08/04

Search for supersymmetry in events with one lepton and multiple jets in proton-proton collisions at $\sqrt{s}$=13 TeV in 2016

The CMS Collaboration

Abstract

A search for supersymmetry is performed in events with a single electron or muon in proton-proton collisions at a center-of-mass energy of 13 TeV in 2016. The data were recorded by the CMS experiment at the LHC, and correspond to an integrated luminosity of 12.9 fb^{-1}. Several exclusive search regions are defined based on the number of jets and b-tagged jets, the scalar sum of the jet transverse momenta, and the scalar sum of the missing transverse momentum and the transverse momentum of the lepton. The observed yields are compatible with predictions from standard model processes. The results are interpreted in two simplified models of gluino pair production. In a model where each gluino decays to top quarks and a neutralino, gluinos with masses up to 1.65 TeV are excluded for neutralino masses below 600 GeV. In the other model, each gluino decays to two light quarks and an intermediate chargino, with the latter decaying to a W boson and a neutralino. Here, gluino masses below 1.6 TeV are excluded for neutralino masses below 500 GeV, assuming a chargino with mass midway between the gluino and neutralino masses.

1 Introduction

Supersymmetry (SUSY) [1–8] is a well-motivated theory beyond the standard model (SM) which provides solutions to several open questions in particle physics, e.g. the cancellation of quadratically divergent loop corrections to the mass of the Higgs boson. In R-Parity [9] conserving SUSY, the lightest SUSY particle (LSP) is stable and can be a viable dark matter candidate.

In this note we present a search for gluino pair production requiring a single lepton and multiple jets. This analysis is based on 13 TeV data recorded in 2016 by the CMS experiment at the CERN LHC, corresponding to an integrated luminosity of 12.9 fb^{-1}. Exclusive search regions are characterized by the number of jets, the number of b-tagged jets, the scalar sum of the transverse momenta p_T of the jets (H_T), and the scalar sum (L_T) of the lepton momentum p_T^ℓ and the imbalance in transverse energy of the event($E_\mathrm{T}^\mathrm{miss}$). The analysis presented here is essentially an application of the analysis described in Ref. [10]. Similar searches were performed in 7 TeV [11–13], 8 TeV [14–16], and 13 TeV [17–19] data by the CMS and ATLAS experiments.

In this analysis, the two main backgrounds are W+jets and top quark antiquark pair ($\mathrm{t\bar{t}}$) events, with one W boson decaying leptonically. The azimuthal angle $\Delta\Phi$ (in radians, in the plane perpendicular to the beam) between the W boson candidate p_T and the lepton p_T is used to separate the signal from these backgrounds. The transverse momentum of the W boson candidate is reconstructed as $p_\mathrm{T}^\mathrm{W} = |\vec{p}_\mathrm{T}^{\,\ell} + \vec{p}_\mathrm{T}^{\,\mathrm{miss}}|$, where $\vec{p}_\mathrm{T}^{\,\mathrm{miss}}$ is defined as the negative vector sum of all reconstructed objects. In particular, in W+jets and semileptonic $\mathrm{t\bar{t}}$ events $\Delta\Phi$ has a maximum value, that is determined by the mass of the W boson and its momentum. The higher the boost of the W boson, the smaller the $\Delta\Phi$ angle, which is given by the requirement of large values of L_T. In SUSY, however, the $E_\mathrm{T}^\mathrm{miss}$ arises not only from the neutrino via the W boson decay, but also from the LSP, leading to a nearly uniform distribution in $\Delta\Phi$. The main backgrounds can therefore be suppressed by rejecting events with a small $\Delta\Phi$ angle. Other backgrounds, such as from $\mathrm{t\bar{t}}$ events where both W bosons decay to a lepton and a neutrino, with one lepton falling out of the experimental acceptance or not reconstructed or identified, also populate the high $\Delta\Phi$ region. Since many models of gluino pair production lead to final states with a large number of jets, the signal-to-background ratio is very small in regions with low jet multiplicity. We therefore restrict the search to regions of large jet multiplicity, and use low jet multiplicity regions, dominantly populated by the background events, to determine the normalization of the background. The multijet background is estimated separately.

The results are interpreted in terms of simplified models [20–23] of gluino pair production. For the first model, called T1tttt in Fig. 1 (left), pair-produced gluinos each decay to a $\mathrm{t\bar{t}}$ pair and the lightest neutralino $\widetilde{\chi}_1^0$. In the other model, termed T5qqqqWW in Fig. 1 (right), the pair-produced gluinos each decay to a quark-antiquark pair of the first or second generation ($\mathrm{q\bar{q}}$), and a chargino $\widetilde{\chi}_1^\pm$ with its mass taken to be $m_{\widetilde{\chi}_1^\pm} = 0.5(m_{\widetilde{\mathrm{g}}} + m_{\widetilde{\chi}_1^0})$; this chargino then decays to a W boson and the $\widetilde{\chi}_1^0$, where the W boson can be virtual, depending on the mass difference between the chargino and the lightest neutralino. Depending on the signal model, the search regions vary in sensitivity.

The organization of this paper is as follows. Section 2 describes the CMS detector. The event reconstruction and selection are discussed in Sections 3 and 4, respectively. The background estimations are given in Section 5. An overview of the main systematic uncertainties is presented in Section 6. The results are discussed and interpreted in Section 7, and a summary is given in Section 8.

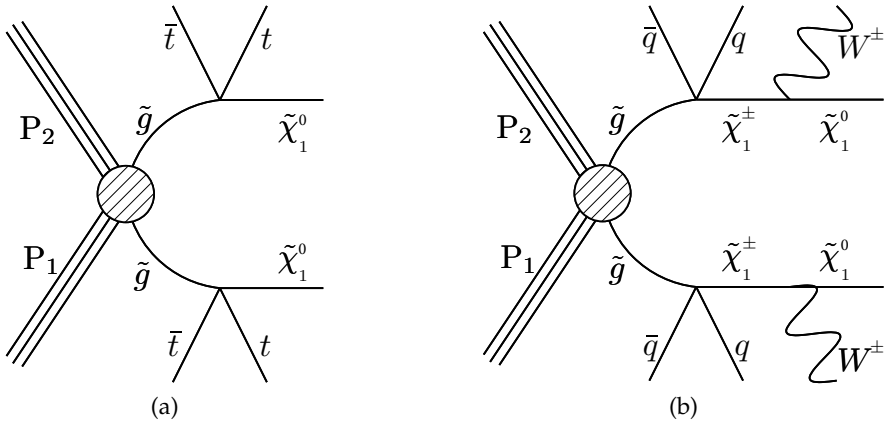

Figure 1: Graphs showing the simplified models (a) T1tttt and (b) T5qqqqWW. Depending on the mass difference between the chargino ($\tilde{\chi}_1^{\pm}$) and the neutralino ($\tilde{\chi}_1^0$), the W boson can be virtual.

2 The CMS detector

The central feature of the CMS apparatus is a superconducting solenoid of 6 m internal diameter, providing a magnetic field of 3.8 T. A silicon pixel and strip tracker, a lead tungstate crystal electromagnetic calorimeter (ECAL), and a brass and scintillator hadron calorimeter (HCAL), each composed of a barrel and two endcap sections, reside within the solenoid volume. Forward calorimeters extend the pseudorapidity (η) [24] coverage provided by the barrel and endcap detectors. Muons are measured in the range $|\eta| < 2.4$, with detection planes made using three technologies: drift tubes, cathode strip chambers, and resistive plate chambers.

The silicon tracker measures charged particles within the range $|\eta| < 2.5$. Isolated particles with transverse momenta $p_{\mathrm{T}} = 100\,\mathrm{GeV}$, emitted at $|\eta| < 1.4$, have track resolutions of 2.8% in p_{T}, and 10 (30) μm in the transverse (longitudinal) impact parameter [25]. The ECAL and HCAL measure energy depositions in the range $|\eta| < 3$, with quartz fibre and steel forward calorimeters extending the coverage to $|\eta| < 5$. When combining information from the entire detector, the jet energy resolutions are typically 15% at 10 GeV, 8% at 100 GeV, and 4% at 1 TeV [26]. The momentum resolution for electrons with $p_{\mathrm{T}} \approx 45\,\mathrm{GeV}$ from $\mathrm{Z} \to \mathrm{ee}$ decays ranges from 1.7% for electrons that do not shower in the barrel region, to 4.5% for electrons that shower in the endcaps [27]. Matching muons to tracks measured in the silicon tracker yields relative transverse momentum resolutions for muons with $20 < p_{\mathrm{T}} < 100\,\mathrm{GeV}$ of 1.3–2.0% in the barrel, and less than 6% in the endcaps. The p_{T} resolution in the barrel is below 10% for muons with p_{T} up to 1 TeV [28].

The CMS trigger system consists of two levels, where the first level (L1), composed of custom hardware processors, uses information from the calorimeters and muon detectors to select the most interesting events in a fixed time interval of less than 4 μs. The high-level trigger (HLT) processor farm further decreases the event rate from around 100 kHz to less than 1 kHz, before data storage.

A more detailed description of the CMS detector, together with a definition of the coordinate system used and the relevant kinematic variables, can be found in Ref. [24].

3 Event reconstruction and simulation

All objects in the event are reconstructed using the particle-flow event reconstruction algorithm [29, 30], that reconstructs and identifies each individual particle through an optimized combination of information from the various elements of the CMS detector. The energy of electrons is determined from a combination of the electron momentum at the primary interaction vertex as determined by the tracker, the energy of the corresponding ECAL cluster, and the energy sum of all bremsstrahlung photons spatially compatible with originating from the electron track [27]. Electron candidates are required to satisfy identification criteria designed to suppress contributions from misidentified jets, photon conversions, and electrons from heavy-flavor quark decays. Muons are reconstructed using a stand-alone muon track in the muon system serving as a seed to find a corresponding track in the silicon detector [28]. Additional criteria include requirements on the track and hit parameters. For both electrons and muons, the requirements are loosened for the identification of additional (vetoed) leptons with high efficiency.

An isolation variable is defined as the p_{T} sum of all objects within a cone around the lepton candidate (excluding the candidate itself), which reflects the activity around the object. An area correction is applied to remove the contribution from additional proton-proton interactions within the same or neighboring bunch crossings (pileup). To enhance the acceptance of signal events that contain a large amount of hadronic energy, we use a p_{T}-dependent cone radius of $R = (0.2,\ 10\,\mathrm{GeV}/p_{\mathrm{T}}[\,\mathrm{GeV}],\ 0.05)$ for $(p_{\mathrm{T}} < 50\,\mathrm{GeV},\ 50\,\mathrm{GeV} < p_{\mathrm{T}} < 200\,\mathrm{GeV},\ p_{\mathrm{T}} > 200\,\mathrm{GeV})$, respectively. This isolation variable, divided by the lepton p_{T} is defined as the relative isolation, and is required to be < 0.4 for vetoed leptons, and less than < 0.2 and < 0.1 for selected muons or electrons, respectively.

The energy of charged hadrons is determined from a combination of their momentum measured in the tracker and the matching ECAL and HCAL energy depositions, corrected for zero-suppression effects in the readout electronics, and for the response function of the calorimeters to hadronic showers. Finally, the energy of neutral hadrons is obtained from the corresponding corrected ECAL and HCAL energies.

Jets are clustered with the anti-k_{t} algorithm with a distance parameter of 0.4 [26]. Jet momentum is determined as the vectorial sum of all particle momenta in the jet. An offset correction is applied to jet energies to take into account the contribution from pileup [31]. Jet energy corrections are obtained from simulation, and are confirmed with in situ measurements of the energy balance in dijet and photon+jet events [26]. Additional selection criteria are applied to each event to remove spurious jet-like features originating from isolated noise patterns in certain HCAL regions.

To discriminate jets originating from b quarks, we use the inclusive combined secondary vertex tagger [32, 33], which employs both secondary vertex and track-based information. The working point is chosen to have about 70% b tagging efficiency and a 1.5% light-flavor misidentification rate [34]. Double counting of objects is avoided by not considering jets that lie within a cone of 0.4 around a lepton.

While the main backgrounds are determined from data, as described in Section 5, simulated events are used to validate the techniques, and to estimate extrapolation factors as needed. In addition, some smaller backgrounds are estimated entirely from simulation. The leading-order (LO) MADGRAPH5 [35] event generator, using the NNPDF3.0LO [36] parton distribution functions (PDFs) is used to simulate $\mathrm{t\bar{t}}$, W+jets, Z+jets, and multijet events. Single-top quark events in the t and tW channels are generated using the next-to-leading order (NLO) POWHEGv1.0 [37–

41] program, and in the s channel using NLO MADGRAPH5_aMC@NLO [42], both along with the NNPDF3.0NLO [36] PDF. All signal events are generated with MADGRAPH5, with up to two partons in addition to the gluino pair. The gluino decays are based on a pure phase-space matrix element [43], with signal production cross sections [44–48] computed at NLO plus next-to-leading-logarithm (NLL) accuracy.

Showering and hadronization of all partons uses the LO PYTHIA 8.2 package [43]. Pileup is generated for some nominal distribution of the number of proton-proton interactions per bunch crossing, which is weighted to match the corresponding distribution in data. The detector response for all backgrounds is modelled using the GEANT4 [49] package, while for the signal the CMS fast simulation program [50] is used to reduce computation time.

4 Trigger and event selection

The events are selected by the HLT requiring an isolated lepton (electron or muon) with p_T of at least 15 GeV, in combination with an online reconstructed H_T of at least 350 GeV or 400 GeV, depending on the instantaneous luminosity. The HLT is seeded by the L1 trigger satisfying $H_T^{L1} > 150$ GeV. An efficiency of 96%(92%)$\pm$1% is observed for the electron (muon) channel in the kinematic regime of the analysis, defined by lepton $p_T > 25$ GeV and $H_T > 500$ GeV.

The electron or muon candidate is required to have a minimum p_T of 25 GeV. Events with additional electrons or muons with $p_T > 10$ GeV, satisfying the criteria for vetoed leptons, are rejected. Jets are selected with $p_T > 30$ GeV and $|\eta| < 2.4$. In all search regions we require at least five jets, where the two hardest jets have to satisfy $p_T > 80$ GeV.

To separate possible new-physics signals from background, we use the L_T variable, which reflects the "leptonic" energy scale of the event. A minimum L_T of 250 GeV is required, such that the analysis is not only sensitive to events with high E_T^{miss}, but also to signal events with very small E_T^{miss}, but higher lepton p_T. An additional kinematic quantity important for the search is given by the "hadronic" energy scale of the event in the form of the variable H_T. For the required $H_T > 500$ GeV, the trigger efficiency reaches its maximum.

Several search regions are defined in bins of n_{jet}, n_b, L_T, and H_T, where n_{jet} and n_b are the numbers of jets and b-tagged jets, respectively. Defining search bins in b-jet multiplicity enables the analysis to target specific event topologies and to separate them from SM backgrounds. The phase space is separated into exclusive [0, 1, 2, $\geq$3] b-tagged jet categories when defining search bins, with a minimum b-jet p_T of 30 GeV.

All search bins with at least one b-tagged jet, called in the following "multi-b", are sensitive to the simplified T1tttt model, while the search bins requiring zero b-tagged jets, called "zero-b", are sensitive to the simplified T5qqqqWW model. The baseline selection and the background estimation method differ for these two b-tag categories. For T1tttt, we expect a large number of jets and find in simulation that the n_{jet} distribution peaks at eight jets for most mass points. We require at least six jets for the multi-b analysis and define two independent categories with n_{jet} = 6–8 and $n_{jet} \geq 9$. For the zero-b analysis, where the T5qqqqWW model has fewer jets, we require in the search region 5, 6–7, or $\geq$8 jets. Depending on the specific SUSY particle masses, the hadronic event activity varies. To accommodate this, we define search bins in H_T. To exploit the strong separation power associated with the L_T variable, we divide the search region in several bins in L_T as well.

After these selections, the main backgrounds are leptonically decaying W+jets and semi-leptonic $t\bar{t}$ events. These backgrounds, both of which contain one lepton and one neutrino (from the W

boson decay) in the final state, are mostly located at small $\Delta\Phi$ values due to the correlation between the lepton and the neutrino. Therefore, the region with large $\Delta\Phi$ is defined as the search region, while the events with small $\Delta\Phi$ are used as the control sample. Figure 2 shows the $\Delta\Phi$ distributions for the zero-b and multi-b search regions. The ratio of search to control region is determined from the sideband with smaller n_{jet}, as described in Section 5. Since the angle between the W boson and the lepton depends on the W momentum, being smaller for W bosons with higher boost, the $\Delta\Phi$ requirement for the signal region is chosen depending on L_{T}, which is a measure of the W boson p_{T}. For the zero-b analysis, $\Delta\Phi$ is required to be larger than 1.0 for most regions except for those with large L_{T}, where the requirement is relaxed to 0.75, while the multi-b analysis has a relaxed $\Delta\Phi$ requirement of 0.75 and 0.5 for medium- and high-L_{T} regions, respectively. In total, we define 30 search bins in the multi-b analysis and 20 search bins in the zero-b analysis, as described in detail in Table 1.

Table 1: Search regions and the corresponding minimum $\Delta\Phi$ requirements.

n_{jet}	n_{b}	L_{T} [GeV]	H_{T} [GeV]	$\Delta\Phi$ [radians]
[6,8]	$= 1, = 2, \geq 3$	$[250, 350]$	$[500, 750]$, ≥ 750	1.0
		$[350, 450]$	$[500, 750]$, ≥ 750	0.75
	$= 1, \geq 2$	$[450, 600]$	$[500, 1250]$, ≥ 1250	
		≥ 600	$[500, 1250]$, ≥ 1250	0.5
≥ 9	$= 1, = 2$	$[250, 350]$	$[500, 1250]$, ≥ 1250	1.0
	≥ 3		≥ 500	
	$= 1, = 2, \geq 3$	$[350, 450]$	≥ 500	0.75
	$= 1, \geq 2$	≥ 450	≥ 500	
5	0	$[250, 350]$, $[350, 450]$	$[500, 750]$, ≥ 750	1.0
		≥ 450	$[500, 750]$, $[750, 1000]$, ≥ 1000	0.75
[6,7]		$[250, 350]$, $[350, 450]$	$[500, 750]$, ≥ 750	1.0
		≥ 450	$[500, 750]$, $[750, 1000]$, ≥ 1000	0.75
≥ 8		$[250, 350]$, $[350, 450]$	$[500, 750]$, ≥ 750	1.0
		≥ 450	$[500, 1000]$, ≥ 1000	0.75

5 Background estimation

The dominant backgrounds in this analysis are $\mathrm{t\bar{t}}$ and W+jets events, with relative yields depending on the multiplicity of b-tagged jets and the kinematic region. To determine these backgrounds, we define two regions for each bin in L_{T}, H_{T}, and n_{b}: the search region (SR) with large values of $\Delta\Phi$, and the control region (CR) with low values of $\Delta\Phi$, with the explicit separation requirement depending on the L_{T} value, as shown in Table 1. We further divide each of these bins into low-n_{jet} sideband (SB) and high-n_{jet} main band (MB) regions.

About 10–15% of the SM background events in the SB are expected to be multijet events (denoted in the following as QCD), and are predicted as described in Section 5.3. Since the multijet background is negligible in the MB, it is subtracted from the number of background events in the SB when calculating the transfer factor $R_{\text{CS}}^{\text{data}}$ to extrapolate from CR (low-$\Delta\Phi$) to SR (high-$\Delta\Phi$). This transfer factor $R_{\text{CS}}^{\text{data}}$ is determined from data in the low-n_{jet} SB regions, separately for each L_{T}, H_{T}, and most n_{b} search region:

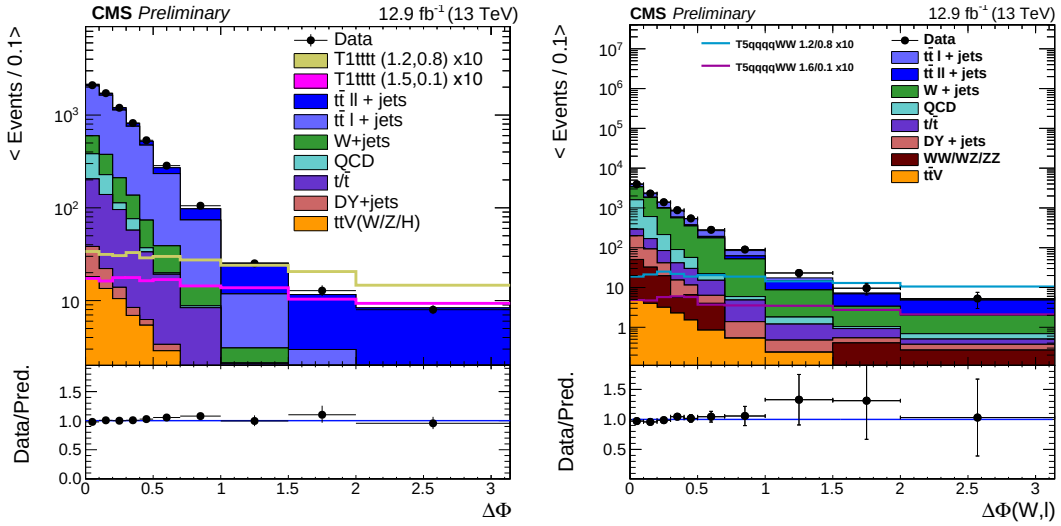

(a) (b)

Figure 2: Comparison of the $\Delta\Phi$ distribution for (a) the multi-b and (b) the zero-b analysis after the baseline selection. The simulated background contributions are stacked on top of each other, and several signal points are overlaid for illustration, but without stacking. For the multi-b analysis, the models T1tttt(1.2,0.8) (T1tttt(1.5,0.1)) correspond to a gluino mass of 1.2 TeV (1.5 TeV) and neutralino mass of 0.8 TeV (0.1 TeV), respectively. For the zero-b analysis, the models T5qqqqWW(1.2,0.8) (T5qqqqWW(1.6,0.1)) correspond to a gluino mass of 1.2 TeV (1.6 TeV) and neutralino mass of 0.8 TeV (0.1 TeV), and the intermediate chargino mass is fixed at 1.0 TeV (0.85 TeV), respectively. The DY refers to $q\bar{q} \rightarrow Z\gamma^* \rightarrow \ell^+\ell^-$ events, and QCD refers to multijet events. The ratio of data to simulation is given below each of the panels. All uncertainties are statistical only.

$$R_{CS}^{data} = \frac{N_{data}^{SB}(SR)}{N_{data}^{SB}(CR) - N_{QCD\ pred}^{SB}(CR)} \quad , \tag{1}$$

where $N_{data}^{SB}(SR)$ is the number of events in the low-n_{jet} SB high-$\Delta\Phi$ signal region, $N_{data}^{SB}(CR)$ the number of events in the low-n_{jet} SB low-$\Delta\Phi$ control region, and $N_{QCD\ pred}^{SB}(CR)$ the predicted number of QCD multijet events in the SB CR.

To account for possible differences in this extrapolation from SB to MB as a function of jet multiplicity, we define multiplicative correction factors κ, determined from simulation.

In the regions with one b tag and four or five jets, about 80% $t\bar{t}$ events and 15–20% W+jets and single top quark events are expected, while in all other multi-b regions, $t\bar{t}$ background is completely dominant. Having only one SM background that dominates, a single R_{CS} factor is defined in the multi-b analysis for each L_T, H_T, and n_b range. With the requirement of having no b-tagged jets, both W+jets and $t\bar{t}$ appear to be of equal importance. Here, an extension of the multi-b strategy is employed, which takes into account differences in the R_{CS} values for these two backgrounds.

An overview of the (n_{jet}, n_b) regions used in this analysis is given in Table 2.

Table 2: Overview of the definitions of sideband and mainband regions. For the multijet (QCD) fit the electron (e) sample is used, while for the determination (det.) of $R_{CS}(W^{\pm})$ the muon (μ) sample is used.

Analysis	Multi-b analysis		Zero-b analysis	
	$n_b = 0$	$n_b \geq 1$	$n_b = 0$	$n_b = 1$
$n_{jet} = 3$	QCD bkg. fit (e sample)		$R_{CS}(W^{\pm})$ det. (μ sample), QCD bkg. fit (e sample)	
$n_{jet} = 4$		R_{CS} det.		$R_{CS}(t\bar{t})$ det.
$n_{jet} = 5$			MB	
$n_{jet} \geq 6$		MB		

5.1 The R_{CS} method for $n_b \geq 1$

For the multi-b analysis, the SB region, where R_{CS} is determined, is required to have four or five jets, while the MB region must satisfy $n_{jet} \in [6-8]$ or $n_{jet} \geq 9$. The predicted number $N^{MB}_{pred}(SR)$ of background events in each MB SR is then given by:

$$N^{MB}_{pred}(SR) = R^{data}_{CS} \cdot \kappa_{EW} \cdot \left[N^{MB}_{data}(CR) - N^{MB}_{QCD\ pred}(CR) \right] \quad , \tag{2}$$

with

$$\kappa_{EW} = \frac{R^{MC}_{CS}(MB, EW)}{R^{MC}_{CS}(SB, EW)} \quad . \tag{3}$$

Here R^{data}_{CS} is the transfer factor determined from data in the low-n_{jet} SB region, and $N^{MB}_{data}(CR)$ is the number of data events in the CR of the MB region. The label EW refers to all backgrounds other than multijets. The residual difference of the values of R_{CS} between the SB and MB regions is evaluated in simulation as the correction factor κ_{EW} given by Eq. (3), where $R^{MC}_{CS}(MB, EW)$ is the R_{CS} in a search MB region from simulation and $R^{MC}_{CS}(SB, EW)$ is the R_{CS} in the corresponding SB region in simulation for the EW background.

The κ_{EW} factor is determined separately for each search bin, except that an overall κ_{EW}-factor is applied for the $n_b \geq 2$ search bins with the same H_T and L_T, since the κ_{EW} factors are found to be nearly independent of n_b. Similarly, R_{CS} at very high H_T is determined jointly across all three n_b bins to increase the number of events, as the overall uncertainty of the background prediction for several of the search bins is dominated by the statistical uncertainty of the yield in the CR of the main band.

Two aspects play a role when R_{CS} is compared between SB and MB: the relative fraction of a certain background, and its corresponding R_{CS} value. For semileptonic $t\bar{t}$ and W+jets events, which contain both one neutrino from the hard interaction, R_{CS} typically has values of 0.01 to 0.04, depending on the search bin. In events with more than one neutrino, e.g. in $t\bar{t}$ events in which both W bosons decay leptonically, R_{CS} is higher with values of around 0.5. This is visible in Fig. 2, where at high $\Delta\Phi$ a large fraction of events is due to dileptonic $t\bar{t}$ background, while the low-$\Delta\Phi$ region is dominated by events with only one neutrino. A larger R_{CS} is also expected for events with three neutrinos, such as $t\bar{t}Z$, when the $t\bar{t}$ system decays semileptonically and the Z boson decays to two neutrinos. The influence of these latter processes is small, since their relative contribution to the background is minor. Most of the SRs with six or more jets are dominated by semileptonic $t\bar{t}$ events, and therefore this background dominates the total R_{CS} value of $\approx$0.05. As the R_{CS} for dileptonic $t\bar{t}$ events is an order of magnitude larger than for semileptonic $t\bar{t}$ events, a slight change in composition in the CR from low- to high-n_{jet}

multiplicity translates into κ_{EW} slightly different from unity. This change in the dileptonic $t\bar{t}$ contribution is accounted for by assigning an uncertainty on the n_{jet} extrapolation based on a dileptonic control sample in data, as discussed in Section 6.

5.2 The R_{CS} method for $n_b = 0$

For search bins where b-tagged jets are vetoed, the background contributions from W+jets and $t\bar{t}$ events are estimated by applying the R_{CS} method separately to each of the two components. This strategy implies the use of two sidebands enriched in W+jets and $t\bar{t}$ events, respectively. For each L_T and H_T bin we denote the n_{jet} SR by n_{jet}^{SR} and write the total background in this SR (with a $\Delta\Phi$ requirement as shown in Table 1) as:

$$N_{MB}^{SR}(0b) \quad = \quad N_{W}^{SR}(0b) + N_{t\bar{t}}^{SR}(0b) + N_{other}^{SR(MC)}(0b) \, , \tag{4}$$

where the number of predicted W+jets and $t\bar{t}$ events is denoted by N_{W}^{SR} and $N_{t\bar{t}}^{SR}$, respectively. Additional backgrounds from rare sources are estimated from simulation and denoted by $N_{other}^{SR(MC)}$.

The expected number of events for each of the components can be described by:

$$N_i^{SR} = N_{data}^{CR} \cdot f_i \cdot R_{CS}^i \, , \text{ with } i = [W, t\bar{t}] \, , \tag{5}$$

where N_{CR}^{data} is the total number of events in the CR of the MB region and f_i is the relative yield of component i. The relative contributions of the two components are determined by a fit of templates obtained from simulation to the n_b multiplicity distribution in the CR of the MB region. The contribution of the QCD multijet background in the CR is fixed to the yield estimated from data as described in Section 5.3. The contribution of other rare background components is obtained from simulation here as well, as is done in the SR. Uncertainties in these two components are propagated as systematic uncertainties to the final prediction. Examples of these fits are shown in Fig. 3.

Two R_{CS} values for W+jets and $t\bar{t}$ are measured in two low n_{jet} SB regions. For the $t\bar{t}$ estimate a sideband with the requirements $4 \leq n_{jet} \leq 5$ and $n_b = 1$ is used. The $R_{CS}^{t\bar{t}}$ is then given by:

$$R_{CS}^{t\bar{t}}(0b, n_{jet}^{SR}) = \kappa_b \cdot \kappa_{t\bar{t}} \cdot R_{CS}^{data}(1b, \, n_{jet} \in [4,5]) \quad . \tag{6}$$

The correction factor κ_b corrects for a potential difference of $R_{CS}^{t\bar{t}}$ between samples with zero or one b jet and for the small contributions of backgrounds other than $t\bar{t}$ or QCD multijet events. The factor $\kappa_{t\bar{t}}$ corrects for a residual dependence of $R_{CS}^{t\bar{t}}$ on n_{jet}, in analogy to the κ_{EWK} factor defined in Section 5.1. Both values, κ_b and $\kappa_{t\bar{t}}$, are close to unity, and statistical uncertainties from the simulation are propagated to the predicted yields.

Similarly, the W+jets contribution is estimated using R_{CS} values from a sideband with $3 \leq n_{jet} \leq 4$ and $n_b = 0$. With respect to the SB used for the estimate of $R_{CS}^{t\bar{t}}$ a lower jet multiplicity is chosen in order to limit the contamination from $t\bar{t}$ events. Only the muon channel is used since it has a negligible contamination from QCD multijet events, contrary to the electron channel. A systematic uncertainty is derived from simulation to cover potential differences between the μ and the combined e and μ samples. The R_{CS}^{W} is given by:

$$R_{CS}^{W}(0b, \, n_{jet}^{SR}) = \kappa_W \cdot R_{CS}^{data(corr)}(0b, \, n_{jet} \in [3,4]) \, . \tag{7}$$

Again, the factor κ_W corrects for a residual dependence of R_{CS}^{W} on the jet multiplicity. The raw value of R_{CS}^{data} measured in the SB has to be corrected for the contamination of $t\bar{t}$ events. The $t\bar{t}$ yields are subtracted in the numerator and denominator according to:

$$R_{CS}^{data(corr)}(0b, n_{jet} \in [3,4]) = \frac{N_{data}^{SR} - R_{CS}^{t\bar{t},MC} \cdot f_{t\bar{t}} \cdot N_{data}^{CR}}{(1 - f_{t\bar{t}}) \cdot N_{data}^{CR}} \,. \tag{8}$$

The event yields N_{data}^{CR} and N_{data}^{SR} are measured in the SB CRs and SRs. The fraction of $t\bar{t}$ events $f_{t\bar{t}}$ is again obtained by a fit to the n_b multiplicity in the SB CR. The R_{CS} value for $t\bar{t}$ in this SB is obtained from simulation.

Systematic uncertainties are assigned to $\kappa_{t\bar{t}}$ and κ_W according to the difference between the R_{CS} values in the sideband and the result of a linear fit over the full range of n_{jet}.

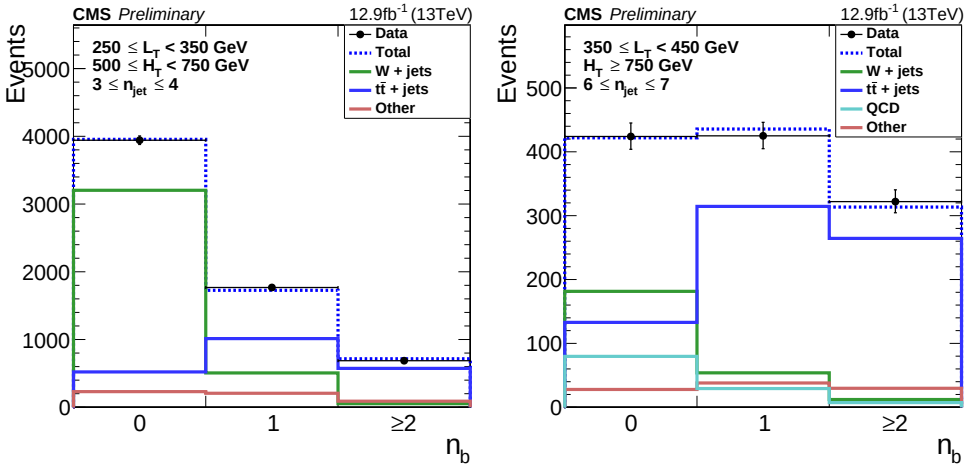

(a) $3 \leq n_{jet} \leq 4$ (b) $6 \leq n_{jet} \leq 7$

Figure 3: Fits to the n_b multiplicity for control regions in (a) $3 \leq n_{jet} \leq 4$ ($250 \leq L_T < 350\,GeV$, $H_T \geq 500\,GeV$, $\Delta\Phi < 1$, muon channel) and (b) $6 \leq n_{jet} \leq 7$ ($250 \leq L_T < 350\,GeV$, $H_T \geq 750\,GeV$, $\Delta\Phi < 1$) in data. The solid lines represent the templates scaled according to the fit result (blue for $t\bar{t}$, green for W+jets, turquoise for QCD, and red for the remaining backgrounds), the dashed line shows the sum after fit, and the points with error bars represent data.

5.3 Estimate of multijet background

Multijet events enter this analysis mostly when reconstructed electrons originate from misidentified jets or from photon conversion in the inner detector. This background is estimated from the yield of 'antiselected' electron candidates in each region, that pass looser identification and isolation requirements, and fail the tighter criteria for selected electrons. These events are scaled by the ratio of jets misidentified as electrons that pass the tight electron identification requirements to the number of antiselected electron candidates in a multijet-enriched control sample with no b-tagged jets and three or four other jets. The assumption is that this sample is devoid of genuine prompt electrons. The estimation method was introduced previously [11, 51], and relies on the L_P variable:

$$L_P = \frac{p_T^{\ell}}{p_T^{W}} \cos(\Delta\Phi) \,, \tag{9}$$

which reflects the effective lepton polarization in the W decay. Its falling distribution between 0 and 1 is well known for SM backgrounds, such as $\mathrm{t\bar{t}}$ and W+jets, while multijet events have a distribution that peaks near $L_\mathrm{P} = 1$.

The ratio of selected to antiselected electron candidates is obtained from a fit to the L_P distribution in bins of L_T. The shape of the QCD multijet contribution used in the fit is taken from the antiselected sample, while the shape of all other contributions is taken from simulation, as the behavior due to W polarization is well understood. The ratios are found to be in the range 0.1–0.2.

In principle, the background estimation with the R_CS method requires knowledge of the multijet contribution in the SR and CR separately. Since the multijet background estimation is performed inclusively with respect to $\Delta\Phi$, an R_CS factor for multijet events is determined as well. In practice, since the resulting R_CS values are all found to be below 2%, the multijet contamination is negligible for the SR. Therefore, the previously described R_CS method takes into account only the QCD multijet contribution in the CR, as written in Eq. (1). For the muon channel, the contribution from QCD multijet background is typically of the order of 1% of the total background. To estimate this contribution, a procedure similar to the one outlined above is applied, and assigned a 100% uncertainty.

6 Systematic uncertainties

Systematic uncertainties either influence κ, and thereby the predictions for the background, or modify the expected signal yield.

The main systematic uncertainty in this analysis is due to the extrapolation of R_CS from the low-n_jet SB to the MB regions of higher jet multiplicities. The ratio of the semileptonic to dileptonic $\mathrm{t\bar{t}}$ final states for different numbers of reconstructed jets is of major importance, since the total R_CS is based on the fraction of the two channels and their corresponding R_CS values, which differ significantly in $\mathrm{t\bar{t}}$ events. To ensure that the data are described well by simulation, a high-purity dilepton $\mathrm{t\bar{t}}$ control sample is selected from the data by requiring two leptons of opposite charge. For same-flavor leptons it is also required that the invariant mass of the lepton pair be more than 10 GeV away from the Z boson mass peak. To simulate the feed-down of the dileptonic events into the single-lepton selection, one of the two leptons is removed from the event. Since these "lost leptons" are principally from $\tau \to$ hadrons + ν decays, we replace the removed lepton by a jet with 2/3 of the original lepton's p_T to accommodate for the missing energy due to the neutrino from the τ decay, and recalculate the L_T, $\Delta\Phi$, and H_T values of the now "single-lepton" event. In order to maximize the number of events, no $\Delta\Phi$ requirement is applied, and all events are used twice, with each reconstructed lepton being considered as the lost lepton. The jet multiplicity distribution after the single-lepton baseline selection (excluding the SRs) and the dilepton CRs are then compared to the simulation. The ratio between data and simulation as a function of n_jet shows in general the same behavior, with the ratio of these two ratios of data over simulation being consistent with unity within statistical uncertainty. The systematic uncertainty in the description of the n_jet distribution in simulation is determined from this double ratio, and is mainly due to the uncertainty of the data samples, which is with 8-40% larger than the observed slope of the double ratio vs. n_jet.

The remaining uncertainties are smaller than the one from the dileptonic $\mathrm{t\bar{t}}$ fraction. In particular, the jet energy scale (JES) is changed by its uncertainty [26] as a function of jet p_T and η, and these changes are propagated to $E_\mathrm{T}^\mathrm{miss}$. The scale factors applied to the efficiencies for the identification of b-quark jets and for the misidentification of c-quark, light-quark or gluon jets

are scaled up and down according to their uncertainties [33]. Uncertainties for the efficiency of lepton reconstruction and identification are handled in the same way. For pileup, a 5% uncertainty on the inelastic cross section [52] is used to obtain its impact on the uncertainty in the pileup. In a few bins with low number of simulated events, the reweighting leads to a large uncertainty.

All these uncertainties apply to both the background prediction and the signal yield. The luminosity is measured with the pixel cluster counting method, and the absolute luminosity scale calibration is derived from an analysis of Van der Meer scans performed in August 2015, resulting in an uncertainty of 6.2% [53].

The W and $\mathrm{t\bar{t}}$ cross sections are changed by 30% to cover possible biases in the estimation of the background composition in terms of W+jets vs. $\mathrm{t\bar{t}}$ events. These changes have only a small impact on the zero-b analysis, where the relative fraction of the two processes is determined from a fit. Also, the following changes in the simulation are performed, with differences between the values of κ in the reweighted and original samples defining the uncertainties. Motivated by measurements at $\sqrt{s} = 8\,\mathrm{TeV}$, simulated $\mathrm{t\bar{t}}$ events are reweighted by a factor $\sqrt{F(\mathrm{t}) \cdot F(\bar{\mathrm{t}})}$, with $F = \min(0.5, \exp\left(0.156 - 0.00137 \cdot p_{\mathrm{T}}^{\mathrm{t}}\right))$, to improve the modelling of the top quark p_{T} spectrum [54]. The reweighting preserves the normalization of the sample, and the difference relative to the results obtained with the unweighted sample is assigned as a systematic uncertainty. The polarization of W bosons is changed by reweighting events by the factor $w = 1 + \alpha(1 - \cos\theta^*)^2$, where θ^* is the angle between the charged lepton and W boson in the W boson rest frame. In W+jets events, we take α to be 0.1, guided by the theoretical uncertainty and measurements found in Refs. [51, 55–57]. For $\mathrm{t\bar{t}}$ events, we take $\alpha = 0.05$. For W+jets events, where the initial state can have different polarizations for $\mathrm{W^+}$ vs. $\mathrm{W^-}$ bosons, we take as uncertainty the larger change in κ resulting from reweighting only the $\mathrm{W^+}$ bosons in the sample, and from reweighting all W bosons. The $\mathrm{t\bar{t}V}$ cross section is changed by 100%. The systematic uncertainty on the multijet estimation depends on n_{jet} and n_{b}, and ranges from 25% to 100%.

For the zero-b analysis, an additional systematic uncertainty is applied, based on linear fits of R_{CS} as a function of n_{jet} as described in Section 5.2, and a 50% cross section uncertainty is used for all backgrounds other than W+jets, $\mathrm{t\bar{t}}$, $\mathrm{t\bar{t}V}$, and multijets.

For the signal, a reweighting procedure is applied based on the number of initial-state radiation (ISR) jets. These weights and the corresponding uncertainties are dervied from $\mathrm{t\bar{t}}$ events, and then propagated to our signal model. The factorization and renormalization scale are each changed by a factor of 0.5 and 2. Uncertainties in the signal cross section are also taken into account.

Additionally, the signal acceptance is corrected for potential resolution effects on the modeling of $E_{\mathrm{T}}^{\mathrm{miss}}$ within the fast simulation software used for the reconstruction of the signal models. The uncertainties based on this correction are propagated as well.

The impact of the systematic uncertainties on the total background prediction for the multi-b and zero-b analyses are summarized in Table 3. While the systematic uncertainty is determined for each signal point, the uncertainties typical for most signals are summarized for illustration in Table 4.

Table 3: Summary of systematic uncertainties in the total background prediction for the multi-b and for the zero-b analysis.

Source	Uncertainty for multi-b [%]	Uncertainty for zero-b [%]
Dilepton control sample	3.4–24	7.5–30
JES	0.3–18	0.7–26
Tagging of b-jets	0.1–3.0	0.7–3.0
σ(W+jets)	0.3–9.3	$<$2.5
W polarization	0.1–3.3	0.7–13.8
$\sigma(\mathrm{t\bar{t}V})$	0.1–4.9	0.1–3.8
Reweighting of top quark p_{T}	0.1–15	0.4–9.3
Pileup	0.4–7.1	0.1–19.6
R_{CS} fit	–	3.2–33.2
Total	8.0–28	9.7–50.6
Statistical uncertainty in MC events	5–30	5.2–35.9

Table 4: Summary of the systematic uncertainties and their average effect on the yields of the benchmark signals. The values are very similar for the multi-b and the zero-b analysis, and are usually larger for compressed scenarios, where the mass difference between gluino and neutralino is small.

Source	Uncertainty [%]
Trigger	1
Pileup	5
Lepton efficiency	5
Luminosity	6.2
ISR	3-20
Tagging of b-jets (heavy flavors)	1-6
Tagging of b-jets (light flavors)	2-3
JES	3-25
Factorization/renormalization scale	<3
$E_{\mathrm{T}}^{\mathrm{miss}}$	3-20
Total	8-33

7 Results and interpretation

The result of the background prediction, the observed data, and the expected numbers of background events from simulation are shown in Fig. 4 and Table 5 for the multi-b, and in Fig. 5 and Table 6 for the zero-b events. The data agrees with SM expectations and no significant excess is observed.

To set limits, a likelihood function for the multi-b or zero-b analysis is formed to contain Poisson probability functions for all four data regions to determine the background in the MB SR. In addition, the κ values from simulation are included to correct any residual differences between the SB and MB regions, with uncertainties incorporated through log-normal constraints. The estimated contribution from multijet events in the two CRs is also included. A profile likelihood ratio in the asymptotic approximation [58] is used as the test statistic. Limits are then calculated at the 95% confidence level (CL) using the asymptotic CLs criterion [59, 60].

The cross section limits obtained for the T1tttt model using the multi-b analysis, and for the T5qqqqWW model using the zero-b analysis, are shown in Fig. 6 as a function of $m(\widetilde{\mathrm{g}})$ and $m(\widetilde{\chi}_1^0)$, assuming branching fractions of 100% as shown in Fig. 1. Using the $\widetilde{\mathrm{g}}\widetilde{\mathrm{g}}$ pair production

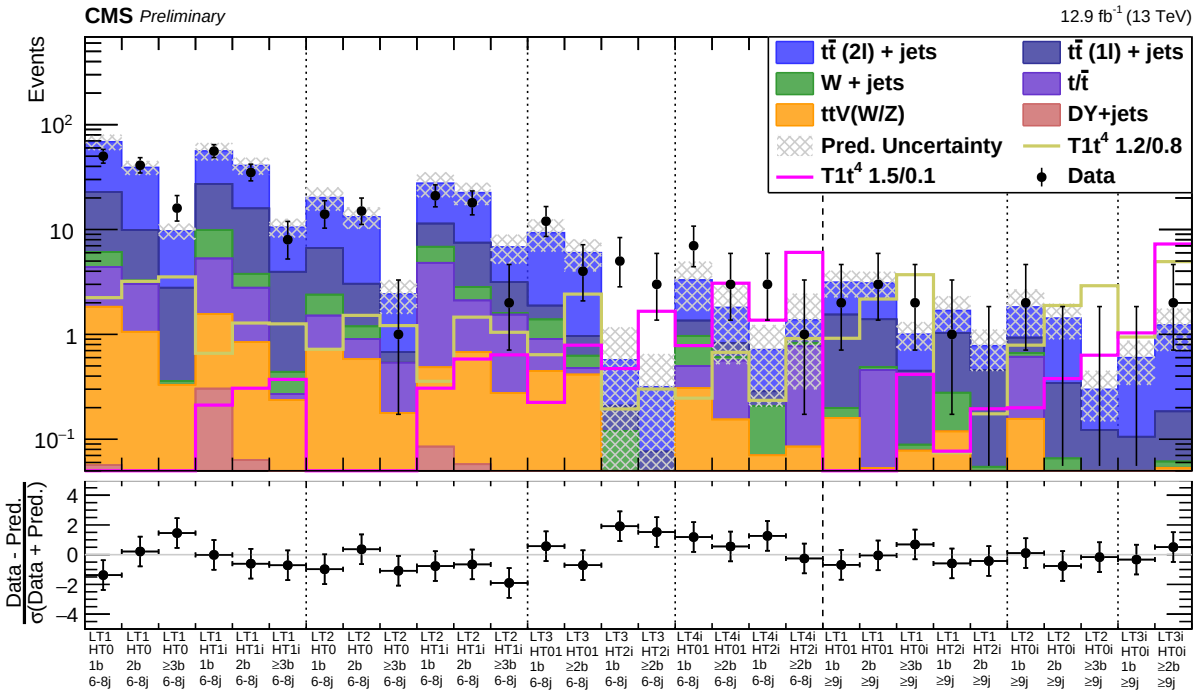

Figure 4: Multi-b search: observed and predicted event counts in the 30 search regions. The black points with error bars show the number of events observed in data. The total expected contribution from standard model background processes is determined from control samples in the data and is used to set the overall normalization of the stacked background histograms. The relative fraction of the individual background components is taken from simulation and shown for illustration only. The uncertainty on the background prediction is shown as a grey, hatched region. The expected event yields for two T1tttt benchmark SUSY models are represented by open histograms. The vertical dashed and dotted lines separate different n_{jet} and L_{T} bins, respectively. The lower panel shows the ratio of the difference between data and background to the sum of the uncertainties on data and background prediction. The error bars indicate the total statistical and systematic uncertainty in the ratio.

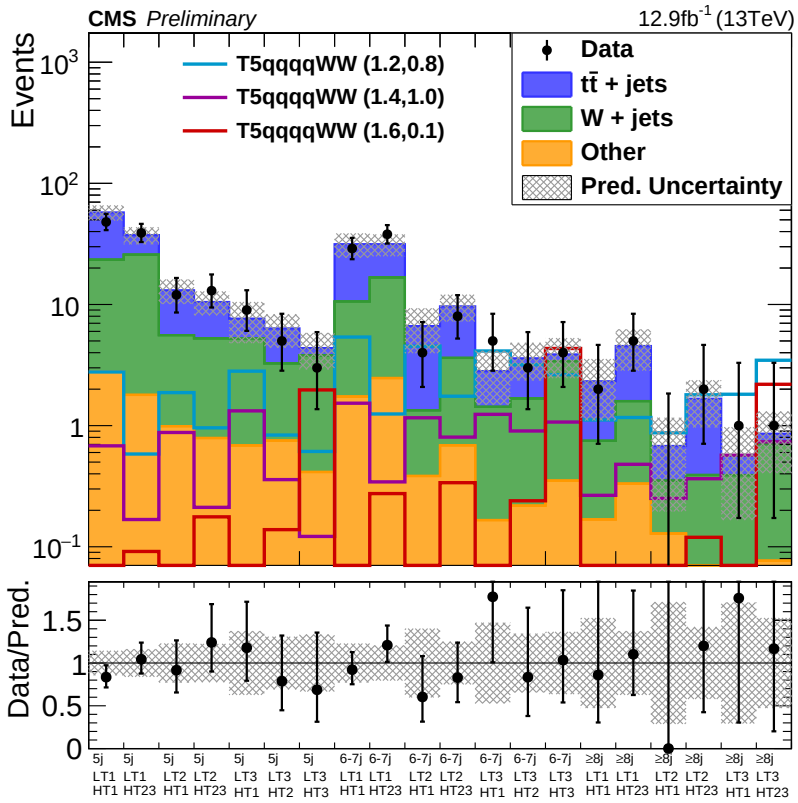

Figure 5: Zero-b search: observed and predicted event counts in the 20 search regions. The black points with error bars show the number of observed events. The background components are shown as stacked histograms. The contributions from $t\bar{t}$ and W+jets are both estimated from control samples in the data. The uncertainty on the background prediction is shown as a grey, hatched region. The expected event yields for three T5qqqqWW benchmark SUSY models are represented by open histograms. The lower panel shows the ratio of data to background prediction. The grey, hatched area indicates the total statistical and systematic uncertainty on the prediction, while the black error bars correspond to the uncertainty on data.

Table 5: Summary of the results in the multi-b search.

$6 \leq n_{jet} \leq 8$							
L_T [GeV]	H_T [GeV]	n_{b-jet}	binName	T1tttt 1.5/0.1	T1tttt 1.2/0.8	Predicted background	Observed
[250, 350]	[500, 750]	$= 1$	LT1, HT0, NB1	< 0.01	2.06 ± 0.16	68.73 ± 11.65	50
		$= 2$	LT1, HT0, NB2	0.03 ± 0.01	3.12 ± 0.17	39.13 ± 5.98	41
		≥ 3	LT1, HT0, NB3i	0.03 ± 0.01	3.57 ± 0.17	9.70 ± 1.66	16
	≥ 750	$= 1$	LT1, HT1i, NB1	0.22 ± 0.04	0.62 ± 0.08	56.19 ± 10.71	56
		$= 2$	LT1, HT1i, NB2	0.33 ± 0.04	1.48 ± 0.12	40.82 ± 7.55	35
		≥ 3	LT1, HT1i, NB3i	0.40 ± 0.04	1.26 ± 0.10	10.52 ± 2.13	8
[350, 450]	[500, 750]	$= 1$	LT2, HT0, NB1	0.01 ± 0.00	0.67 ± 0.09	20.15 ± 5.05	14
		$= 2$	LT2, HT0, NB2	0.02 ± 0.01	1.41 ± 0.12	13.21 ± 3.05	15
		≥ 3	LT2, HT0, NB3i	0.04 ± 0.01	1.07 ± 0.09	2.43 ± 0.86	1
	≥ 750	$= 1$	LT2, HT1i, NB1	0.31 ± 0.05	0.41 ± 0.06	27.68 ± 7.40	21
		$= 2$	LT2, HT1i, NB2	0.58 ± 0.06	1.37 ± 0.11	22.48 ± 5.38	18
		≥ 3	LT2, HT1i, NB3i	0.64 ± 0.05	1.10 ± 0.09	6.83 ± 2.11	2
[450, 600]	[500, 1250]	$= 1$	LT3, HT01, NB1	0.24 ± 0.04	0.54 ± 0.07	9.33 ± 3.18	12
		≥ 2	LT3, HT01, NB2i	0.84 ± 0.07	2.15 ± 0.13	6.01 ± 2.03	4
	≥ 1250	$= 1$	LT3, HT2i, NB1	0.49 ± 0.06	0.17 ± 0.04	0.57 ± 0.60	5
		≥ 2	LT3, HT2i, NB2i	1.73 ± 0.10	0.24 ± 0.04	0.32 ± 0.33	3
≥ 600	[500, 1250]	$= 1$	LT4i, HT01, NB1	0.77 ± 0.07	0.23 ± 0.05	3.31 ± 1.64	7
		≥ 2	LT4i, HT01, NB2i	2.97 ± 0.13	0.58 ± 0.07	1.81 ± 1.29	3
	≥ 1250	$= 1$	LT4i, HT2i, NB1	1.35 ± 0.10	0.21 ± 0.05	0.72 ± 0.51	3
		≥ 2	LT4i, HT2i, NB2i	5.84 ± 0.17	0.92 ± 0.08	1.37 ± 1.08	1
$n_{jet} \geq 9$							
L_T [GeV]	H_T [GeV]	n_{b-jet}	binName	T1tttt 1.5/0.1	T1tttt 1.2/0.8	Predicted background	Observed
[250, 350]	[500, 1250]	$= 1$	LT1, HT01, NB1	0.02 ± 0.01	0.83 ± 0.10	3.15 ± 0.90	2
		$= 2$	LT1, HT01, NB2	0.03 ± 0.01	2.13 ± 0.14	3.09 ± 0.87	3
	≥ 500	≥ 3	LT1, HT0i, NB3i	0.44 ± 0.04	3.62 ± 0.16	1.00 ± 0.31	2
	≥ 1250	$= 1$	LT1, HT2i, NB1	0.08 ± 0.03	0.08 ± 0.03	1.69 ± 0.62	1
		$= 2$	LT1, HT2i, NB2	0.21 ± 0.03	0.20 ± 0.04	0.78 ± 0.33	0
[350, 450]	≥ 500	$= 1$	LT2, HT0i, NB1	0.21 ± 0.04	0.81 ± 0.10	1.83 ± 0.86	2
		$= 2$	LT2, HT0i, NB2	0.37 ± 0.05	1.82 ± 0.13	1.43 ± 0.53	0
		≥ 3	LT2, HT0i, NB3i	0.66 ± 0.05	2.67 ± 0.14	0.30 ± 0.15	0
≥ 450	≥ 500	$= 1$	LT3i, HT0i, NB1	1.04 ± 0.08	0.85 ± 0.09	0.60 ± 0.27	0
		≥ 2	LT3i, HT0i, NB2i	7.17 ± 0.18	4.67 ± 0.19	1.23 ± 0.54	2

cross section calculated at next-to-leading order within next-to-leading-logarithmic accuracy, exclusion limits are set as a function of the $(m_{\tilde{g}}, m_{\tilde{\chi}_1^0})$ mass hypothesis.

8 Summary

A search for supersymmetry has been performed with 12.9 fb^{-1} of proton-proton collision data recorded by the CMS experiment at $\sqrt{s} = 13$ TeV in 2016. The data are analyzed in several exclusive categories, differing in the number of jets and b-tagged jets, the scalar sum of all jet transverse momenta, and the scalar sum of the imbalance in transverse momentum and the transverse momentum of the lepton. The main background is significantly reduced by requiring a large azimuthal angle between the directions of the lepton and of the reconstructed W boson p_T. No significant excess is observed, and the results are interpreted in terms of two simplified models that describe gluino pair production.

For a simplified model in which each gluino decays through an off-shell top squark to a $\text{t}\bar{\text{t}}$ pair and the lightest neutralino, gluino masses up to 1.65 TeV are excluded for neutralino masses below 600 GeV. Neutralino masses below 950 GeV can be excluded for a gluino mass of approximately 1.5 TeV. A second simplified model also describes gluino pair production, with the gluinos decaying to first or second generation quarks and a chargino, which then decays to a W boson and the lightest neutralino. The chargino mass in this decay chain is taken to be $m_{\tilde{\chi}_1^\pm} = 0.5(m_{\tilde{g}} + m_{\tilde{\chi}_1^0})$. In this model, gluino masses below 1.6 TeV are excluded for neutralino

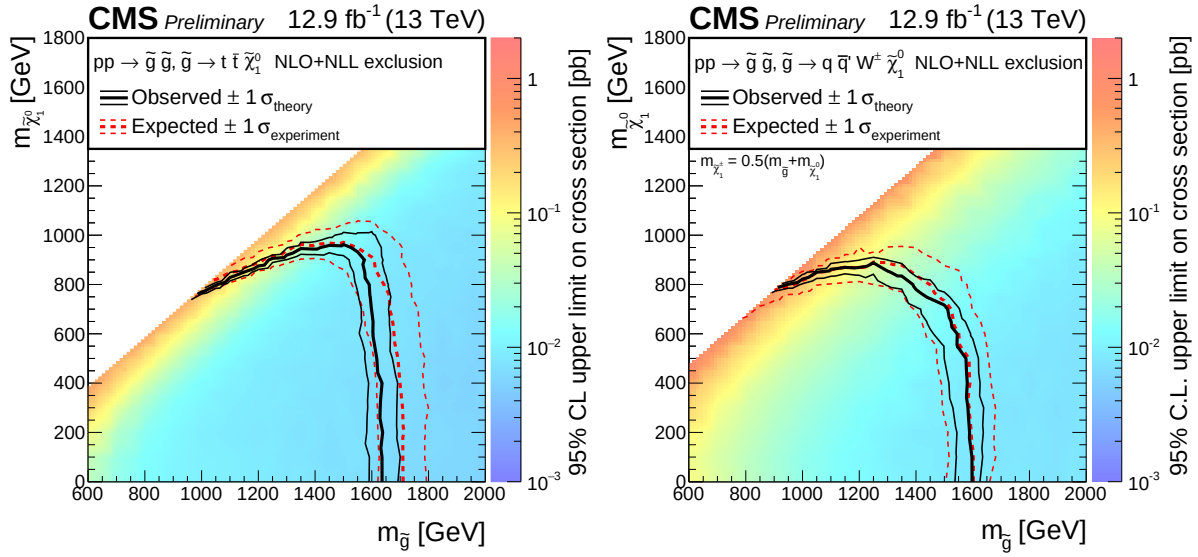

(a) (b)

Figure 6: Cross section limits at a 95% CL for (a) the T1tttt model, and (b) the T5qqqqWW model. For the T5qqqqWW model, the mass of the chargino is taken to be $m_{\tilde{\chi}_1^\pm} = 0.5(m_{\tilde{g}} + m_{\tilde{\chi}_1^0})$. The solid black (dashed red) lines correspond to the observed (expected) mass limits, with the thicker lines representing the central values and the thinner lines representing the $\pm 1\sigma$ uncertainty bands related to the theoretical (experimental) uncertainties.

Table 6: Background prediction and observation in the 0-tag regions, 12.9fb^{-1}

n_{jet}	L_{T} [GeV]	H_{T} [GeV]	Bin name	Expected signal T5qqqqWW $m_{\tilde{g}}/m_{\tilde{\chi}^0}$ [TeV] (1.2/0.8)	(1.4/1.0)	(1.6/0.1)	Predicted background	Observed
5	[250, 350]	[500, 750]	LT1, HT1	2.77 ± 0.58	0.68 ± 0.22	0.01 ± 0.01	57.5 ± 8.29	48
		≥ 750	LT1, HT23	0.58 ± 0.21	0.17 ± 0.09	0.09 ± 0.05	37.38 ± 6.07	39
	[350, 450]	[500, 750]	LT2, HT1	1.87 ± 0.48	0.88 ± 0.24	<0.01	13.1 ± 3.0	12
		≥ 750	LT2, HT23	0.96 ± 0.25	0.21 ± 0.14	0.18 ± 0.07	10.48 ± 2.35	13
	≥ 450	[500, 750]	LT3, HT1	2.82 ± 0.55	1.32 ± 0.28	0.01 ± 0.01	7.64 ± 2.85	9
		[750, 1000]	LT3, HT2	0.84 ± 0.27	0.36 ± 0.13	0.14 ± 0.05	6.35 ± 1.96	5
		≥ 1000	LT3, HT3	0.61 ± 0.23	0.12 ± 0.07	1.97 ± 0.46	4.37 ± 1.46	3
[6, 7]	[250, 350]	[500, 750]	LT1, HT1	5.39 ± 0.87	1.53 ± 0.31	<0.01	31.45 ± 7.18	29
		≥ 750	LT1, HT23	1.25 ± 0.35	0.34 ± 0.16	0.27 ± 0.07	31.44 ± 6.46	38
	[350, 450]	[500, 750]	LT2, HT1	4.53 ± 0.81	1.16 ± 0.28	<0.01	6.63 ± 2.67	4
		≥ 750	LT2, HT23	1.75 ± 0.57	0.8 ± 0.26	0.34 ± 0.08	9.65 ± 2.41	8
	≥ 450	[500, 750]	LT3, HT1	4.13 ± 0.77	1.24 ± 0.29	<0.01	2.82 ± 1.33	5
		[750, 1000]	LT3, HT2	3.18 ± 0.75	0.9 ± 0.28	0.24 ± 0.06	3.59 ± 1.24	3
		≥ 1000	LT3, HT3	2.64 ± 0.63	1.07 ± 0.29	4.33 ± 0.57	3.87 ± 1.41	4
≥ 8	[250, 350]	[500, 750]	LT1, HT1	1.11 ± 0.35	0.27 ± 0.15	<0.01	2.32 ± 1.22	2
		≥ 750	LT1, HT23	1.17 ± 0.36	0.48 ± 0.18	0.04 ± 0.02	4.54 ± 1.69	5
	[350, 450]	[500, 750]	LT2, HT1	0.87 ± 0.28	0.25 ± 0.16	<0.01	0.68 ± 0.48	0
		≥ 750	LT2, HT23	1.8 ± 0.51	0.36 ± 0.15	0.12 ± 0.05	1.67 ± 0.7	2
	≥ 450	[500, 1000]	LT3, HT1	1.82 ± 0.53	0.57 ± 0.21	0.02 ± 0.01	0.57 ± 0.4	1
		≥ 1000	LT3, HT23	3.47 ± 0.97	0.73 ± 0.23	2.19 ± 0.55	0.86 ± 0.45	1

masses below 500 GeV. Neutralino masses below 850 GeV can be excluded for a gluino mass of approximately 1.3 TeV. These results extend the limits obtained from the dataset recorded in 2015 by up to 200 GeV.

References

[1] P. Ramond, "Dual theory for free fermions", *Phys. Rev. D* **3** (1971) 2415, doi:10.1103/PhysRevD.3.2415.

[2] Y. A. Golfand and E. P. Likhtman, "Extension of the algebra of Poincaré group generators and violation of P invariance", *JETP Lett.* **13** (1971) 323.

[3] A. Neveu and J. H. Schwarz, "Factorizable dual model of pions", *Nucl. Phys. B* **31** (1971) 86, doi:10.1016/0550-3213(71)90448-2.

[4] D. V. Volkov and V. P. Akulov, "Possible universal neutrino interaction", *JETP Lett.* **16** (1972) 438.

[5] J. Wess and B. Zumino, "A Lagrangian model invariant under supergauge transformations", *Phys. Lett. B* **49** (1974) 52, doi:10.1016/0370-2693(74)90578-4.

[6] J. Wess and B. Zumino, "Supergauge transformations in four dimensions", *Nucl. Phys. B* **70** (1974) 39, doi:10.1016/0550-3213(74)90355-1.

[7] P. Fayet, "Supergauge invariant extension of the Higgs mechanism and a model for the electron and its neutrino", *Nucl. Phys. B* **90** (1975) 104, doi:10.1016/0550-3213(75)90636-7.

[8] H. P. Nilles, "Supersymmetry, supergravity and particle physics", *Phys. Rep.* **110** (1984) 1, doi:10.1016/0370-1573(84)90008-5.

[9] G. R. Farrar and P. Fayet, "Phenomenology of the production, decay, and detection of new hadronic states associated with supersymmetry", *Physics Letters B* **76** (1978), no. 5, 575 – 579, doi:http://dx.doi.org/10.1016/0370-2693(78)90858-4.

[10] CMS Collaboration, "Search for supersymmetry in events with one lepton in proton-proton collisions at $\sqrt{s} = 13TeV$ with the CMS experiment", CMS Physics Analysis Summary CMS-PAS-SUS-15-006, CERN, 2016.

[11] CMS Collaboration, "Search for supersymmetry in pp collisions at $\sqrt{s} = 7$ TeV in events with a single lepton, jets, and missing transverse momentum", *Eur. Phys. J. C* **73** (2013) 2404, doi:10.1140/epjc/s10052-013-2404-z, arXiv:1212.6428.

[12] CMS Collaboration, "Search for supersymmetry in final states with a single lepton, b-quark jets, and missing transverse energy in proton-proton collisions at $\sqrt{s} = 7$ TeV", *Phys. Rev. D* **87** (2013) 052006, doi:10.1103/PhysRevD.87.052006, arXiv:1211.3143.

[13] ATLAS Collaboration, "Further search for supersymmetry at $\sqrt{s} = 7$ TeV in final states with jets, missing transverse momentum and isolated leptons with the ATLAS detector", *Phys. Rev. D* **86** (2012) 092002, doi:10.1103/PhysRevD.86.092002, arXiv:1208.4688.

[14] CMS Collaboration, "Search for supersymmetry in pp collisions at $\sqrt{s} = 8$ TeV in events with a single lepton, large jet multiplicity, and multiple b jets", *Phys. Lett. B* **733** (2014) 328, doi:10.1016/j.physletb.2014.04.023, arXiv:1311.4937.

[15] ATLAS Collaboration, "Search for squarks and gluinos in events with isolated leptons, jets and missing transverse momentum at $\sqrt{s} = 8$ TeV with the ATLAS detector", *JHEP* **04** (2015) 116, doi:10.1007/JHEP04(2015)116, arXiv:1501.03555.

[16] ATLAS Collaboration, "Search for strong production of supersymmetric particles in final states with missing transverse momentum and at least three b-jets at $\sqrt{s}$= 8 TeV proton-proton collisions with the ATLAS detector", *JHEP* **10** (2014) 024, doi:10.1007/JHEP10(2014)024, arXiv:1407.0600.

[17] CMS Collaboration, "Search for supersymmetry in pp collisions at sqrt(s) = 13 TeV in the single-lepton final state using the sum of masses of large-radius jets", arXiv:1605.04608. Submitted to JHEP.

[18] ATLAS Collaboration, "Search for gluinos in events with an isolated lepton, jets and missing transverse momentum at $\sqrt{s}$ = 13 TeV with the ATLAS detector", arXiv:1605.04285. Submitted to EPJC.

[19] ATLAS Collaboration, "Search for pair production of gluinos decaying via stop and sbottom in events with b-jets and large missing transverse momentum in pp collisions at $\sqrt{s} = 13$ TeV with the ATLAS detector", arXiv:1605.09318.

[20] N. Arkani-Hamed et al., "MARMOSET: The path from LHC data to the new standard model via on-shell effective theories", (2007). arXiv:hep-ph/0703088.

[21] J. Alwall, P. Schuster, and N. Toro, "Simplified models for a first characterization of new physics at the LHC", *Phys. Rev. D* **79** (2009) 075020, doi:10.1103/PhysRevD.79.075020, arXiv:0810.3921.

[22] J. Alwall, M.-P. Le, M. Lisanti, and J. G. Wacker, "Model-independent jets plus missing energy searches", *Phys. Rev. D* **79** (2009) 015005, doi:10.1103/PhysRevD.79.015005, arXiv:0809.3264.

[23] D. Alves et al., "Simplified models for LHC new physics searches", *J. Phys. G* **39** (2012) 105005, doi:10.1088/0954-3899/39/10/105005, arXiv:1105.2838.

[24] CMS Collaboration, "The CMS experiment at the CERN LHC", *JINST* **3** (2008) S08004, doi:10.1088/1748-0221/3/08/S08004.

[25] CMS Collaboration, "Description and performance of track and primary-vertex reconstruction with the CMS tracker", *JINST* **9** (2014) P10009, doi:10.1088/1748-0221/9/10/P10009, arXiv:1405.6569.

[26] CMS Collaboration, "Determination of jet energy calibration and transverse momentum resolution in CMS", *JINST* **6** (2011) P11002, doi:10.1088/1748-0221/6/11/P11002, arXiv:1107.4277.

[27] CMS Collaboration, "Performance of electron reconstruction and selection with the CMS detector in proton-proton collisions at $\sqrt{s} = 8$ TeV", *JINST* **10** (2015) P06005, doi:10.1088/1748-0221/10/06/P06005, arXiv:1502.02701.

[28] CMS Collaboration, "Performance of CMS muon reconstruction in pp collision events at $\sqrt{s} = 7$ TeV", *JINST* **7** (2012) P10002, doi:10.1088/1748-0221/7/10/P10002, arXiv:1206.4071.

[29] CMS Collaboration, "Particle-flow event reconstruction in CMS and performance for jets, taus, and $E_{\mathrm{T}}^{\mathrm{miss}}$", CMS Physics Analysis Summary CMS-PAS-PFT-09-001, CERN, 2009.

[30] CMS Collaboration, "Commissioning of the particle-flow event with the first LHC collisions recorded in the CMS detector", CMS Physics Analysis Summary CMS-PAS-PFT-10-001, CERN, 2010.

[31] M. Cacciari and G. P. Salam, "Pileup subtraction using jet areas", *Phys. Lett. B* **659** (2008) 119, doi:10.1016/j.physletb.2007.09.077, arXiv:0707.1378.

[32] CMS Collaboration, "Identification of b-quark jets with the CMS experiment", *JINST* **8** (2013) P04013, doi:10.1088/1748-0221/8/04/P04013, arXiv:1211.4462.

[33] CMS Collaboration, "Identification of b quark jets at the CMS Experiment in the LHC Run 2", CMS Physics Analysis Summary CMS-PAS-BTV-15-001, CERN, 2016.

[34] CMS Collaboration, "Performance of b tagging at $\sqrt{s} = 8$ TeV in multijet, $\mathrm{t\bar{t}}$ and boosted topology events", CMS Physics Analysis Summary CMS-PAS-BTV-13-001, CERN, 2013.

[35] J. Alwall et al., "MadGraph5: going beyond", *JHEP* **06** (2011) 128, doi:10.1007/JHEP06(2011)128, arXiv:1106.0522.

[36] NNPDF Collaboration, "Parton distributions for the LHC Run II", *JHEP* **04** (2015) 040, doi:10.1007/JHEP04(2015)040, arXiv:1410.8849.

[37] P. Nason, "A new method for combining NLO QCD with shower Monte Carlo algorithms", *JHEP* **11** (2004) 040, doi:10.1088/1126-6708/2004/11/040, arXiv:hep-ph/0409146.

[38] S. Frixione, P. Nason, and C. Oleari, "Matching NLO QCD computations with parton shower simulations: the POWHEG method", *JHEP* **11** (2007) 070, doi:10.1088/1126-6708/2007/11/070, arXiv:0709.2092.

[39] S. Alioli, P. Nason, C. Oleari, and E. Re, "A general framework for implementing NLO calculations in shower Monte Carlo programs: the POWHEG BOX", *JHEP* **06** (2010) 043, doi:10.1007/JHEP06(2010)043, arXiv:1002.2581.

[40] S. Alioli, P. Nason, C. Oleari, and E. Re, "NLO single-top production matched with shower in POWHEG: s- and t-channel contributions", *JHEP* **09** (2009) 111, doi:10.1007/JHEP02(2010)011, 10.1088/1126-6708/2009/09/111, arXiv:0907.4076. [Erratum: JHEP **02** (2010) 011].

[41] E. Re, "Single-top Wt-channel production matched with parton showers using the POWHEG method", *Eur. Phys. J. C* **71** (2011) 1547, doi:10.1140/epjc/s10052-011-1547-z, arXiv:1009.2450.

[42] J. Alwall et al., "The automated computation of tree-level and next-to-leading order differential cross sections, and their matching to parton shower simulations", *JHEP* **07** (2014) 079, doi:10.1007/JHEP07(2014)079, arXiv:1405.0301.

[43] T. Sjöstrand et al., "An Introduction to PYTHIA 8.2", *Comput. Phys. Commun.* **191** (2015) 159, doi:10.1016/j.cpc.2015.01.024, arXiv:1410.3012.

[44] W. Beenakker, R. Höpker, M. Spira, and P. M. Zerwas, "Squark and gluino production at hadron colliders", *Nucl. Phys. B* **492** (1997) 51, doi:10.1016/S0550-3213(97)00084-9, arXiv:hep-ph/9610490.

[45] A. Kulesza and L. Motyka, "Threshold resummation for squark-antisquark and gluino-pair production at the LHC", *Phys. Rev. Lett.* **102** (2009) 111802, doi:10.1103/PhysRevLett.102.111802, arXiv:0807.2405.

[46] A. Kulesza and L. Motyka, "Soft gluon resummation for the production of gluino-gluino and squark-antisquark pairs at the LHC", *Phys. Rev. D* **80** (2009) 095004, doi:10.1103/PhysRevD.80.095004, arXiv:0905.4749.

[47] W. Beenakker et al., "Soft-gluon resummation for squark and gluino hadroproduction", *JHEP* **12** (2009) 041, doi:10.1088/1126-6708/2009/12/041, arXiv:0909.4418.

[48] W. Beenakker et al., "Squark and gluino hadroproduction", *Int. J. Mod. Phys. A* **26** (2011) 2637, doi:10.1142/S0217751X11053560, arXiv:1105.1110.

[49] S. Agostinelli et al., "GEANT4 — a simulation toolkit", *Nucl. Instr. and Meth. A* **506** (2003) 250, doi:10.1016/S0168-9002(03)01368-8.

[50] CMS Collaboration, "The Fast Simulation of the CMS Detector at LHC", Technical Report 3, CERN, 2011.

[51] CMS Collaboration, "Measurement of the Polarization of W Bosons with Large Transverse Momenta in W+Jets Events at the LHC", *Phys. Rev. Lett.* **107** (2011) 021802, doi:10.1103/PhysRevLett.107.021802, arXiv:1104.3829.

[52] ATLAS Collaboration, "Measurement of the Inelastic Proton-Proton Cross Section at $\sqrt{s} = 13$ TeV with the ATLAS Detector at the LHC", (2016). arXiv:1606.02625. Submitted to *PRL*.

[53] CMS Collaboration, "CMS Luminosity Measurement for the 2015 Data Taking Period", CMS Physics Analysis Summary CMS-PAS-LUM-15-001, CERN, 2016.

[54] CMS Collaboration, "Measurement of the differential cross section for top quark pair production in pp collisions at $\sqrt{s} = 8$ TeV", *Eur. Phys. J.* **C75** (2015), no. 11, 542, doi:10.1140/epjc/s10052-015-3709-x, arXiv:1505.04480.

[55] Z. Bern et al., "Left-Handed W Bosons at the LHC", *Phys. Rev.* **D84** (2011) 034008, doi:10.1103/PhysRevD.84.034008, arXiv:1103.5445.

[56] CMS Collaboration, "Angular coefficients of Z bosons produced in pp collisions at $\sqrt{s} = 8$ TeV and decaying to $\mu^+\mu^-$ as a function of transverse momentum and rapidity", *Phys. Lett. B* **750** (2015) 154, doi:10.1016/j.physletb.2015.08.061, arXiv:1504.03512.

[57] ATLAS Collaboration, "Measurement of the polarisation of W bosons produced with large transverse momentum in pp collisions at $\sqrt{s} = 7$ TeV with the ATLAS experiment", *Eur. Phys. J. C* **72** (2012) 2001, doi:10.1140/epjc/s10052-012-2001-6, arXiv:1203.2165.

[58] G. Cowan, K. Cranmer, E. Gross, and O. Vitells, "Asymptotic formulae for likelihood-based tests of new physics", *Eur. Phys. J. C* **71** (2011) 1554, doi:10.1140/epjc/s10052-011-1554-0, 10.1140/epjc/s10052-013-2501-z, arXiv:1007.1727. [Erratum: Eur. Phys. J. C **73** (2013) 2501].

[59] T. Junk, "Confidence level computation for combining searches with small statistics", *Nucl. Instr. and Meth. A* **434** (1999) 435, doi:10.1016/S0168-9002(99)00498-2, arXiv:hep-ex/9902006.

[60] A. L. Read, "Presentation of search results: the CL_s technique", *J. Phys. G* **28** (2002) 2693, doi:10.1088/0954-3899/28/10/313.